



Applied Catalysis B: Environmental

journal homepage: www.elsevier.com/locate/apcatb

Study on the decomposition of trace benzene over V₂O₅–WO₃/TiO₂-based catalysts in simulated flue gas

Sheng-yong Lu^{a,b}, Qiu-lin Wang^a, William R. Stevens^{b,1}, Chun Wai Lee^{b,*}, Brian K. Gullett^b, Yong-xin Zhao^{c,2}

^a State Key Laboratory of Clean Energy Utilization, Institute for Thermal Power Engineering of Zhejiang University, Hangzhou 310027, China

^b US Environmental Protection Agency, Office of Research and Development, National Risk Management Research Laboratory, Research Triangle Park, NC 27711, USA

^c ARCADIS U.S., Inc., 4915 Prospectus Drive, Suite F, Durham, NC 27713, USA

ARTICLE INFO

Article history:

Received 28 February 2013

Received in revised form 29 August 2013

Accepted 30 August 2013

Available online 8 September 2013

Keywords:

Honeycombed catalyst

REMPI-TOFMS

Trace benzene

Simulated flue gas

Raman spectroscopy

ABSTRACT

Catalytic decomposition of benzene was studied by using oxides of vanadium and tungsten supported on titanium oxide (TiO₂) catalysts for effective reduction of emissions of toxic organic compounds from waste incineration. Experiments were conducted to evaluate the effects of the catalyst's composition, and operating conditions on benzene decomposition, and the relationship between molecular structures of catalysts and their activity was also investigated through replacing the conventional TiO₂ catalyst support by nano-sized TiO₂. Trace levels (1 and 10 ppm) of gaseous benzene were catalytically decomposed in a fixed-bed catalytic reactor with monolithic oxides of vanadium and tungsten supported on titanium oxide (V₂O₅–WO₃/TiO₂) catalysts under conditions simulating the cooling of waste incineration flue gas. On-line monitoring of trace benzene concentrations before and after the catalyst was achieved by means of resonance enhanced multiphoton ionization-time of flight mass spectrometry (REMPI-TOFMS). Catalysts were characterized by nitrogen adsorption, X-ray diffraction, energy dispersive X-ray spectroscopy, temperature-programmed reduction, and Raman spectroscopy. The effects of several parameters, including catalyst operating temperature, space velocity (SV) and initial benzene concentration, on catalytic oxidation of benzene were investigated. Experimental results indicate that reduction of the initial benzene concentration from 10 to 1 ppm either enhances or decreases the catalytic removal efficiency depending on the adsorption capability as well as the oxidation ability of the catalyst tested. The catalytic activity for benzene oxidation not simply relies on the vanadium content of the catalyst; the molecular structure of vanadium oxide, which is known to be influenced by both vanadium oxide loading and the type of support, is very important. Nano-sized TiO₂ supported vanadium oxide catalyst (VWNT) with lowest V loading (0.75 wt.%) provides higher catalytic activity than those of the catalysts with higher V contents (1.31 and 2.92 wt.%) but supported by conventional TiO₂ (VWT1 and VWT2). The relatively higher catalytic activity of VWNT may be attributed to: (a) the presence of monomeric VO_x species, with one terminal V=O bond as indicated by Raman spectra; (b) fewer impurities confounding active catalytic constituents (V, W and Ti); (c) pure anatase phase of TiO₂ rather than a mixture phase of anatase and rutile servicing as catalyst support besides its nano-scale particle size; (d) larger specific surface area, smaller average pore diameter, and narrower pore size distribution contribute higher adsorption ability for benzene. No obvious competition effect between NO_x removal and benzene oxidation was observed in this study. Reaction rate constants and activation energies for benzene catalytic oxidation tested by the catalysts were calculated. Lower activation energy obtained from VWNT than those of the two catalysts further confirming the higher catalytic activity of VWNT.

Published by Elsevier B.V.

1. Introduction

Incineration has recently become the preferred waste treatment method for municipal solid waste and medical waste in China, as incineration can quickly reduce waste volume and allow for energy recovery. However, waste incineration development still suffers a variety of societal pressures, due to the poor reputation of incineration resulting from the release of pollutants,

* Corresponding author. Tel.: +1 919 541 7663.

E-mail address: lee.chun-wai@epa.gov (C.W. Lee).

¹ Present address: College of Health Sciences, Kentucky Christian University, 100 Academic Parkway, Grayson, KY 41143, USA.

² Present address: POET Research, Inc, 4615N Lewis Avenue, Sioux Falls, SD 57104, USA.

including particles, the usual combustion by-products (i.e., CO, NO_x, SO_x), and hazardous species (i.e., aromatic compounds and heavy metals). Technically feasible and cost-effective technologies must be developed to minimize the environmental and health impacts of waste incineration. Carcinogenic benzene, which is regulated under stringent emission standards [1], is one of the representative volatile organic compounds (VOCs) frequently found in waste incineration flue gas [2]. Moreover, chlorinated benzene is a precursor of polychlorinated dibenz-p-dioxins and polychlorinated dibenzofurans (PCDDs/Fs), substances of major health concern. Therefore, technical approaches for reducing benzene emissions from waste combustion also have high potential for reducing the environmental impact of waste incineration.

Catalytic oxidation is one of the most important air pollutant control technologies, which can achieve complete destruction of aromatic compounds without creating secondary solid pollutants that require extra disposal [3–5]. Since Hagenmeier [6] first proved that PCDDs/Fs can be effectively converted into CO₂, H₂O, and HCl via TiO₂-supported oxides of vanadium and tungsten (V₂O₅–WO₃/TiO₂) catalyst originally designed for controlling NO_x [7], the V₂O₅–WO₃/TiO₂ catalyst has been studied intensively for complete catalytic oxidation of VOCs [8–13], or PCDDs/Fs [4,6,14,15]. The catalyst was found to have excellent activity and stability by previous studies [16,17], particularly in comparison with other TiO₂-supported transition metal oxides (i.e., CrO_x, CuO_x, MnO_x, CoO_x, MoO_x and FeO_x). Moreover, simultaneous removal of NO_x and PCDDs/Fs was observed to be achievable mainly by promoting the oxidation potential of the catalysts by increasing the vanadium content [4,18]. However, most previous researches were carried out on measurement of the catalytic activity of V₂O₅–WO₃/TiO₂ on laboratory scale experiments and the operating conditions for such experiments are usually quite different from those for industrial scale applications [19]: (1) the concentration levels of the target organic compounds at the inlet of the catalyst are far higher (around 100 ppm) [14,20–22] than the concentration levels in incinerator flue gases due to the limitation of the detection thresholds of the monitoring method; (2) the gas compositions used in the laboratory scale experiments are often simplified to include only oxygen, nitrogen and H₂O [23–26], without considering the influence of NO_x, SO_x, HCl and other organic compounds on the catalytic oxidation processes; (3) the space velocity (SV) may be lower than the actual SV values used in operating systems, resulting in higher catalytic conversion in laboratory-scale experiments; and (4) the catalysts tested are frequently in the form of powders [1,16,27,28] rather than the honeycomb monoliths mostly used in industrial units. As a result of these factors, significantly different operating conditions between laboratory-scale and field-scale tests may produce different test results. Therefore, experimental conditions similar to those of full-scale incineration plants operating in the field were simulated in present work to duplicate practical conditions, providing a strong basis for further research on evaluation of catalysts in actual incinerator plants. Moreover, several key experimental parameters including operating temperature, initial concentration, space velocity, and flue gas components are investigated. Also, influences of catalyst support and catalyst composition, which are the critical factors determining the coupling between support and surface species, on catalyst activity is discussed.

2. Materials and methods

2.1. Catalyst characterization

Three commercial monolithic vanadium oxide catalysts (Zhejiang Sanlong Catalyst Co., Ltd., China) with two supported by conventional TiO₂ (VWT1 and VWT2), and another one (VWNT)

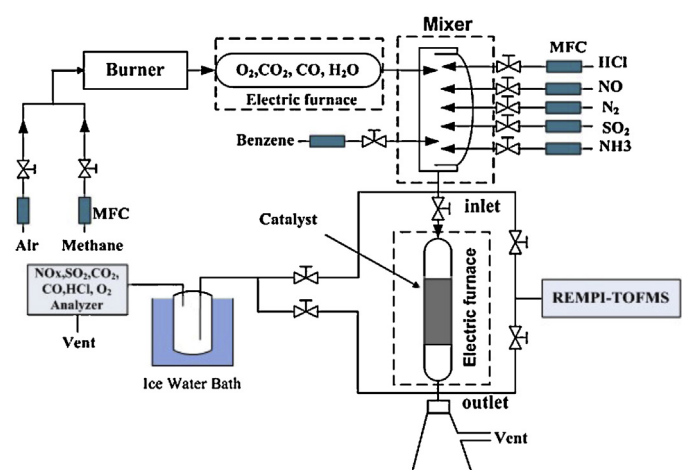


Fig. 1. Schematic diagram of the catalytic decomposition test experimental set-up.

was supported by nano-scale TiO₂ (Degussa P25) were tested in this study. These honeycomb catalysts were crushed to powder before characterization. Specific surface area and pore size distribution of the catalysts were obtained by N₂-sorption equipped with an automated Brunauer–Emmet–Teller (BET) and pore analyzer (TRISTAR 3020, Mike Instrument Co., America). The XRD patterns were determined using a Philips Model XD-98 X-ray diffractometer with CuK α radiation ($\lambda = 0.15406$ nm). The catalyst samples were scanned over the range 10–80° 2 θ at a rate of 0.02°/min. Content of each component in catalysts were obtained by energy dispersive X-ray (EDX) spectroscopy. H₂-temperature-programmed reduction (H₂-TPR) was used to determine the reducibility of catalysts and was implemented for each ca. 100 mg of catalysts from 50 to 700 °C with a Micromeritics Autochem II 2920 equipped with a thermal conductivity detector (TCD). Raman spectroscopy of the samples was performed with LabRamHRUV (JOBINYVON Co., France) equipped with an Ar-ion laser, to study the surface speciation of TiO₂-supported vanadium oxide catalysts. The incident laser was tuned to 514.5 nm and 13 mW of power was delivered at the sample. The samples without further treatment were pressed into self-supporting wafers and the Raman spectra of the catalysts were recorded under ambient conditions.

2.2. Catalyst test system

The catalytic oxidation tests were carried out in a tubular quartz reactor at atmospheric pressure with a honeycomb catalyst insert. The temperature of the reactor was controlled closely with an electric furnace (Fig. 1). Combustion gases (containing CO₂, CO, O₂, and H₂O) generated by a methane burner (controlled at 1000 °C) were mixed with HCl, SO₂, NO, and NH₃ from gas cylinders with concentrations respectively fixed at 50, 400, 300, and 360 ppm to create a simulated waste incineration flue gas atmosphere for the tests. The O₂ and CO₂ measured after the methane burner were 5.0% and 4.8%, respectively and were fed into fixed bed catalytic reactor. Gaseous benzene (provided by a gas cylinder) was doped using a mass flow controller into the simulated flue gas at two different concentrations (1 and 10 ppm). The total gas flow rates through the reactor were controlled at 7 L/min and 14 L/min for establishing SV values of 2000 h⁻¹ and 4000 h⁻¹, respectively. Benzene concentrations, both inflow and outflow of the catalyst, were determined by REMPI-TOFMS which can measure trace gaseous aromatic compounds [29–31] at high sensitivity, selectivity and real time. The flue gas was pulled through heated Teflon and stainless steel lines to the REMPI-TOFMS by a positive displacement pump at a flow rate of 2 L/min. The sample line was heated and maintained at 125 °C using

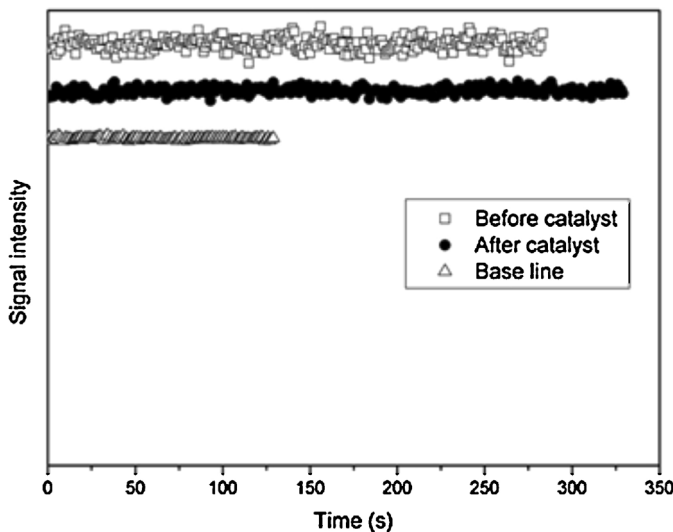


Fig. 2. REMPI-TOFMS signal intensity data plotted over time (catalyst: VWT1; benzene inlet concentration: 10 ppm; T: 350 °C; SV: 2000 h⁻¹).

Type K thermocouples and temperature control units to ensure that none of the target analytes adsorbed to the walls of the line.

To ensure quality of the experimental data, calibration of the REMPI-TOFMS was performed at the beginning and the end of each daily testing period in two steps: checking the wavelength output of the laser system and converting the peak area measured in the REMPI-TOFMS spectra (signal intensity, I) to benzene concentration. The signal intensity data recorded per second by REMPI-TOFMS before and after the catalyst as well as the baseline data recorded before the test are shown in Fig. 2. The relative standard deviations of the data shown in Fig. 2 were calculated and are listed in Table 1. A range of relative standard deviations between 0.33 and 1.49% was identified, confirming the stability of the detection data from REMPI-TOFMS. The catalytic removal efficiency (η_b) of benzene reported in this study is calculated according to Eq. (1), based on the average baseline signal intensity (I_{baseline}) from REMPI-TOFMS accompanied by the signal intensity before (I_{inlet}) and after (I_{outlet}) the catalyst:

$$\eta_b = \frac{I_{\text{catalyst inlet}} - I_{\text{catalyst outlet}}}{I_{\text{catalyst inlet}} - I_{\text{baseline}}} \quad (1)$$

The data imported into Eq. (1) are the averages of the signal intensity values obtained from a period of 5 min sampling.

3. Results and discussion

3.1. Characteristics of $V_2O_5-WO_3/TiO_2$ catalysts

The compositions and structure parameters of the tested commercial catalysts, including two conventional TiO_2 -supported (VWT1, VWT2) and one nano- TiO_2 supported V_2O_5/WO_3 catalysts (VWNT), are shown in Table 2. In comparison with VWT1 and VWT2, VWNT with least V loading (0.8 wt.%) and most Ti content (52.9 wt.%) has largest BET surface area (166 m²g⁻¹) which is almost a factor of two larger than those of VWT1 and VWT2 (approximately

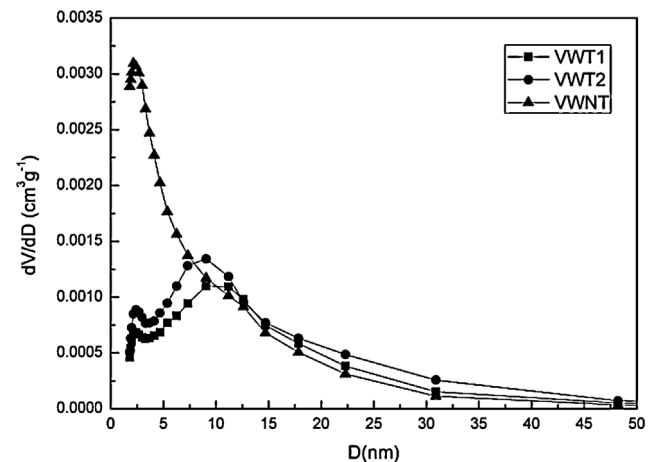


Fig. 3. Pore size distributions of the catalysts.

75 m²g⁻¹ for VWT1 and 88 m²g⁻¹ for VWT2), suggesting a better dispersion of surface active species. Although all three catalysts are abundant in mesopores (2–50 nm), the pore size distribution of VWNT is quite different from those of VWT1 and VWT2 as shown in Fig. 3. The majority of the pore size in VWNT is located in pores with diameters less than 5 nm. However, the pore sizes of the other two catalysts are distributed in the range from 7 to 12 nm, which is consistent with the results displayed in Table 2, VWT1 and VWT2 share almost the same average pore diameters but they are much larger than that of VWNT. Moreover, extra attention should be paid to the fact that impurities are abundant in VWT1 and VWT2, reaching up to 10.8 and 43.0 wt.% respectively while the Ti contents in these two catalysts are hence reduced accordingly. By contrast, VWNT contains fewer impurities (2.6 wt.%) and appears to be much "cleaner".

The XRD patterns of VWT1, VWT2, and VWNT are shown in Fig. 4. From the pattern of VWNT, only peaks corresponding to anatase TiO_2 appear, indicating anatase TiO_2 is the predominant phase, and V_2O_5 is in either amorphous or microcrystalline forms which are insufficient to be detected from this catalyst [32]. As for VWT1, a small peak assigned to rutile TiO_2 is also found in its XRD pattern besides anatase phase peaks. However, as observed from pattern b of VWT2, a small peak attributed to the diffraction by crystalline V_2O_5 (2θ = 20.3°) is detected. Moreover, several small peaks corresponding to $MnTiO_3$ and Mn_2O_3 are also observed in VWT2 because of the impurities introduced in the catalyst during catalyst preparation.

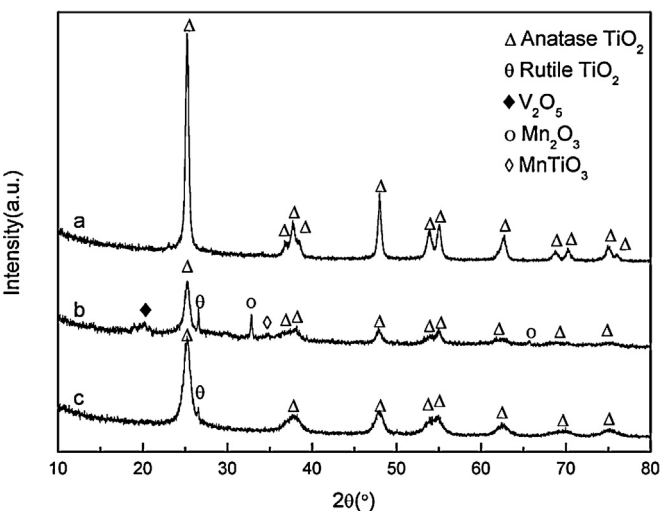


Fig. 4. XRD patterns of the catalysts: (a) VWNT, (b) VWT2 and (c) VWT1.

Table 1

Relative standard deviation of the REMPI-TOFMS measurement data.

Sampling points	Before the catalyst	After the catalyst	Baseline
Relative standard deviation (%)	1.49	0.95	0.33

Table 2

Summary of the components and the structure parameters of the catalysts.

Notation	Main components	V (wt.%)	W (wt.%)	Ti (wt.%)	O (wt.%)	Others ^a (wt.%)	$S_{\text{BET}}^{\text{b}}/(\text{m}^2 \text{g}^{-1})$	$V_{\text{tot}}^{\text{b}}/(\text{cm}^3 \text{g}^{-1})$	D^{b}/nm
VWT1	$\text{V}_2\text{O}_5\text{--WO}_3/\text{TiO}_2$	1.3	6.1	44.0	37.8	10.8	75	0.21	10.6
VWT2	$\text{V}_2\text{O}_5\text{--WO}_3/\text{TiO}_2$	2.9	5.2	13.2	35.7	43.0	88	0.25	10.4
VWNT	$\text{V}_2\text{O}_5\text{--WO}_3/\text{Nano-TiO}_2$	0.8	6.0	52.9	37.8	2.6	166	0.27	6.6

^a Impurities introduced during these commercial monolithic catalyst preparation process, including Si, Mg, Al, Mn, Fe, Ca, K, S elements.^b S_{BET} : BET specific surface area; V_{tot} : total pore volume; D : average pore diameter.

Recently, Raman spectroscopy has been widely applied to examine molecular structures of supported metal oxide catalysts and obtain insight into the reaction mechanism of heterogeneous catalysis [33–36]. Fig. 5 shows the Raman spectra of the three catalysts. It was reported [37,38] that the anatase TiO_2 possessing Raman peaks at ~ 395 , ~ 511 and $\sim 633 \text{ cm}^{-1}$, which are all measured in both VWT1 and VWNT and those peaks observed from VWNT are more intense. As can be seen from the Raman spectrum of VWNT, the vibration at $\sim 1030 \text{ cm}^{-1}$ arising from the symmetric stretch of a mono-oxo terminal V=O bond of isolated surface vanadium species ($\text{support-O}_3\text{-V=O}$) is present [39,40]. Comparison with the literature data revealed that the broader Raman band at $\sim 930 \text{ cm}^{-1}$ originates from the vibrations of V, O and Ti ions, which indeed is resulted from the strong V–O-support interactions [41], is also appeared in the case of VWNT. These observations for VWNT may be attributed to the well dispersion of vanadium on catalyst surface resulting from its less V loading as well as its larger BET surface area. Accordingly, the possible molecular structure of supported vanadia surface species in VWNT is depicted in Fig. 5d: an isolated tetrahedral vanadium oxide species consisting of a single V=O terminal bond and three V–O-support bonds [42]. As for VWT1 and VWT2, no visible peaks attributed to V=O , V–O–V or even crystalline V_2O_5 (vibration at $\sim 998 \text{ cm}^{-1}$) are observed. The absence of Raman signals assigned to interactions between V, O and the support in VWT1 and VWT2 is probably ascribed to the disturbance of strong bonds from TiO_2 support and the fluorescence which probably be induced by the impurities introduced in the catalysts during preparation. Especially for VWT2, which contains most impurities (43.0 wt.%) and leads to only one tiny peak at $\sim 633 \text{ cm}^{-1}$ attributed to TiO_2 as observed from its Raman spectrum.

H_2 -temperature-programmed reduction ($\text{H}_2\text{-TPR}$) is frequently used to investigate the reducibility of the catalysts. Fig. 6 shows $\text{H}_2\text{-TPR}$ profiles of the catalysts. As for VWNT catalyst, a broad peak rising from ca. 100°C to 550°C and a second peak centered

at around 678°C are found. According to the observation of vanadium-based catalyst in previous reports [43,44], these TPR profiles are respectively assigned to the reductions of V^{5+} species and W^{6+} species. Whereas, the peaks attributed to the reduction of vanadia from V^{5+}O_x to V^{3+}O_x , centering at 457°C and 553°C respectively for VWT1 and VWT2, are much sharper and are shifted to higher temperature regions compared to the VWNT peak. The peak observed from VWNT is less sharp than those of the two other catalysts, which may be due to the relatively lower V content of VWNT. However, this reduction peak is also much broader and starts from a lower temperature (ca. 100°C), which suggests that VWNT is easier to provide oxygen atom to react with H_2 and thus have better activity at relatively lower temperature than the other two catalysts.

3.2. Catalytic activity evaluation

The three honeycombed catalysts showed different catalytic activities toward benzene oxidation as the results presented in Fig. 7. Previous research suggests that commercial vanadium-based ($\text{V}_2\text{O}_5\text{--WO}_3/\text{TiO}_2$) catalyst can be optimized for combining PCDD/F destruction and NO_x reduction, mainly by promoting the oxidation potential of the catalyst by increasing the catalyst's vanadium content [3]. However, the VWNT catalyst with the lowest V content in this study showed consistently higher benzene removal efficiency than the other two catalysts, indicating that the V content of the catalyst may not be the sole factor determining the catalytic activity of the vanadium oxide-based catalysts. Nevertheless, molecular structures of the supported vanadium oxide, which are mainly influenced by both the choice of catalyst support and V content, are also pivotal for catalyst activity. Schimmoeller et al. [45] suggested that not all VO_x species present on the catalyst surface would be responsible for the catalytic activity, but that the V–O–V bonds in close proximity to the catalyst support (TiO_2) could be considered as the most active species. According to previous studies [46,47],

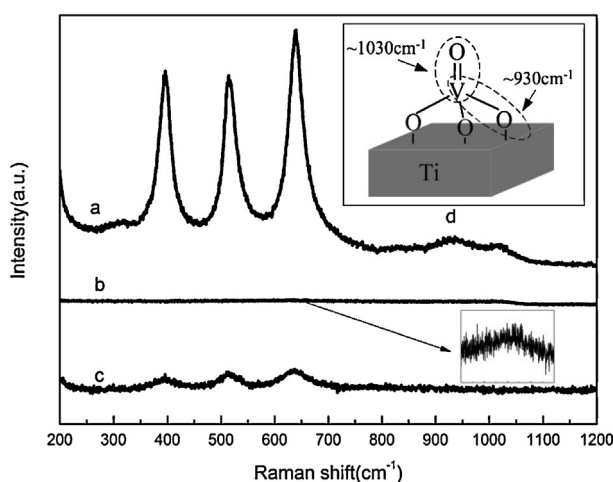


Fig. 5. Raman spectra of (a) VWNT, (b) VWT2, (c) VWT1 and (d) possible molecular structure of supported vanadia surface species in VWNT.

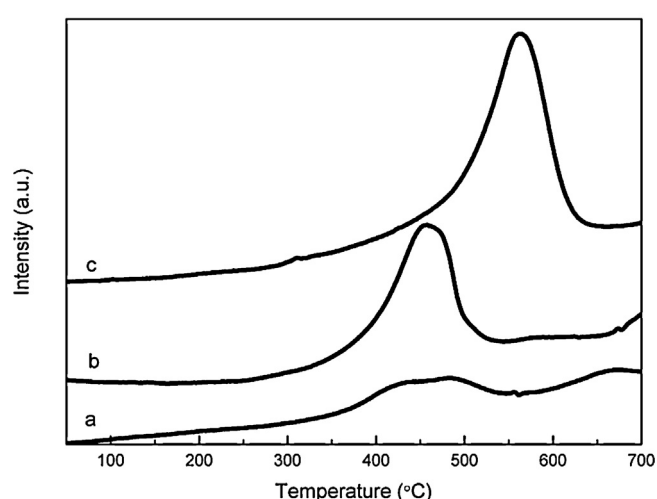


Fig. 6. $\text{H}_2\text{-TPR}$ profiles of (a) VWNT, (b) VWT1 and (c) VWT2.

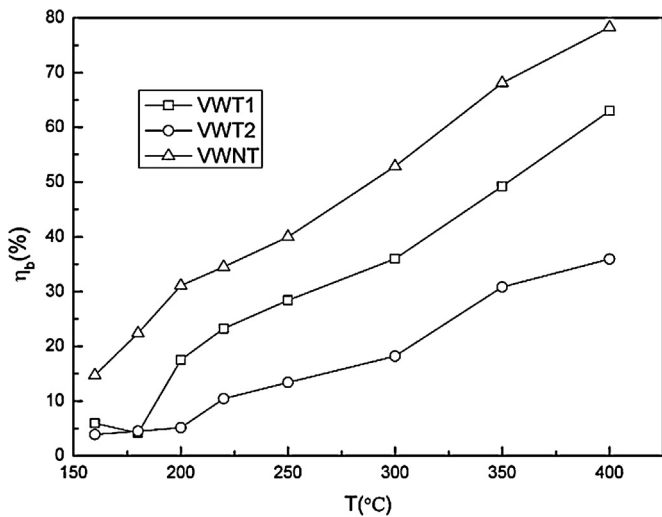


Fig. 7. Benzene removal efficiencies achieved with VWNT, VWT1 and VWT2, respectively, at different operating temperatures (SV: 2000 h⁻¹; initial concentration: 10 ppm).

a strong support effect on the turnover frequency of the methanol oxidation reaction was observed and which can be explained as an indication that the V–O-support bonds are likely to be the active centers. Interestingly, VWNT which contains V=O and V–O–Ti bonds (shown in Fig. 5d) as confirmed by Raman spectroscopy also showed better catalytic performance in this work. However, VWT1 and VWT2, whose vibrations of vanadium oxide internal bonds are too weak to be detected, exhibited relatively lower catalytic activities. These observations are consistent with the suggestions that the formed surface species such as V=O groups and V–O–Ti bonds are closely related with the catalyst activity and have been deemed the active sites in supported vanadia catalysts [41,42,48]. Therefore, nano-TiO₂ can be served as a better catalyst support from this aspect compared to conventional TiO₂, because the former optimizes the dispersion of vanadium oxide and enhances the bonding between vanadium and catalyst support on VWNT. It should be noted that catalysts tested in this study are commercial monolithic catalysts; impurities are often introduced during their preparation in the form of adhesive, agent and lubricant used for honeycomb catalyst extrusion. These additives remain in the monolithic catalysts and squeeze out some of the catalyst active ingredients, possibly leading to the reduction of catalyst activity. VWT2 which has highest V content (2.9 wt.%) but lowest Ti content (13.2 wt.%) exhibits lowest catalyst activity. In fact, VWNT which has least other impurities (only 2.6 wt.%) hence contains most active components and performs best in catalytic oxidation of benzene. For this reason, additive contents have noticeable negative effect on catalytic activity. Therefore, it is suggested that only small amount of additives is allowed during monolithic catalyst preparation to maintain the high activity of the catalyst. Furthermore, it is commonly believed that anatase phase TiO₂ is more suitable to be the catalyst support than the rutile phase TiO₂ [49,50], which performs better than the rutile phase in photocatalysis [51]. As indicated by XRD profiles, the only phase detected for nano-TiO₂ in VWNT is anatase, while a mixture of anatase and rutile phases are observed for conventional TiO₂ in both VWT1 and VWT2. The interesting structural differences between these two kinds of TiO₂ supports also demonstrate the benefit of the anatase phase being served as the catalyst support. This may be another main advantage for the nano-TiO₂ support besides its nano-scale particle size.

Heterogeneous catalytic processes happen only after the successful capture of gaseous pollutants onto the catalyst surface,

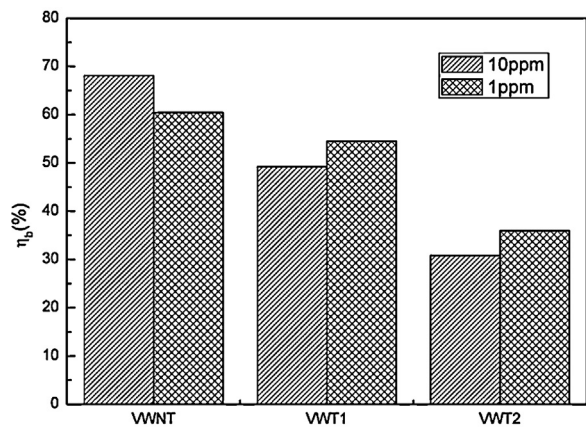


Fig. 8. Benzene removal efficiencies achieved with VWNT, VWT1 and VWT2, respectively, at different initial concentrations (SV: 2000 h⁻¹; T: 350 °C).

indicating that adsorption ability, besides oxidation ability of the catalyst, is also important for benzene removal. Previous studies observed that gaseous organic compound adsorption takes place mainly in the pore, whose diameter is close to the diameter of the molecular size of the organic compound, so that the adsorption potential is higher due to the proximity of the pore walls [52,53]. The size of the benzene molecule is approximately 0.74 nm. Therefore, VWNT with comparatively larger S_{BET} (166 m² g⁻¹, as listed in Table 2), smaller average pore diameter (6.56 nm), and narrower pore size distribution (abundance of pores of diameter 2–5 nm, closer to the benzene molecular size) possesses higher adsorption ability for benzene, which is possibly another reason for higher catalytic activity. The effects of benzene initial concentrations (1 ppm and 10 ppm) and space velocities (2000 h⁻¹ and 4000 h⁻¹) on benzene catalytic oxidation were also studied. As shown in Fig. 8, the influence of benzene inlet concentrations was rather nebulous in this case: increasing benzene inlet concentration from 1 ppm to 10 ppm increased benzene catalytic removal efficiency from 60% to 68% for VWNT. Conversely, when the catalysts were VWT1 and VWT2, removal efficiencies decreased. In general, increasing the benzene inlet concentration increases the competition between benzene molecules for active sites on the catalyst surface, which may lower the benzene catalytic removal efficiency when the catalyst provides insufficient active sites. However, if sufficient active sites are available, catalytic removal efficiency is determined mainly by the destruction rate of reactants on active sites, instead of probability of collision between benzene molecules and active sites, explaining why different effects of initial benzene concentration were observed from VWNT, VWT1 and VWT2 in Fig. 8, which is also an indication of the number of effective active sites on the three catalysts are reduced in the order: VWNT > VWT1 > VWT2. Taking the V content of each catalyst into account can further confirm that not all VO_x species on catalyst surface to form effective active sites, but VO₄ specie with one terminal V=O bond and anchored by three Ti–O–V bonds to Ti support (pyramidal-type structure as shown in Fig. 5d) can be considered as the effective active sites which are absent from the Raman spectra of VWT1 and VWT2.

Fig. 9 presents the removal efficiencies of benzene at different space velocities achieved with VWNT. The result indicates that the percentage of benzene being removed is reduced significantly as the space velocity is increased, probably due to the shorter benzene retention time on the catalyst, reducing the effective collisions between benzene molecules and catalytic active sites, leading to reduction of removal efficiency at higher space velocities.

Catalytic decomposition of benzene must undergo three main processes: (1) adsorption–target organic compounds adsorb onto

Table 3

Benzene removal efficiency in different flue gas components (initial concentration = 5 ppm; SV = 2000 h⁻¹; T = 400 °C).

Catalysts	Benzene removal efficiency in different flue gas components (%)			
	Simulated flue gas	No NH ₃	No NH ₃ /NO	No NH ₃ /NO/HCl/SO ₂
VWNT	78.9	78.1(−0.8) ^a	78.6(−0.3)	78.1(−0.8)
VWT1	57.5	55.6(−1.9)	57.5(+0.0)	57.1(−0.4)
VWT2	31.3	30.3(−1.0)	29.8(−1.5)	32.4(+1.1)

^a The numbers in brackets refer to the variation of benzene removal efficiency (%) after switching off the valves of NH₃, NO, HCl and SO₂ one by one.

the catalyst surface; (2) destruction–adsorbed compounds are activated and then oxidized by the oxygen atom in the active sites; and (3) desorption–decomposition products desorb from the surface. In the case of VWNT, sufficient active sites are available as indicated by the influence of benzene initial concentration, thus catalytic removal efficiency is determined mainly by the destruction rate of reactants on active sites with extremely low inlet benzene concentrations (<10 ppm) relative to those of other reacting species. All reactive species, including benzene, NH₃ and NO molecular, are subjected to the active sites on the catalyst surface in this work. The destruction of benzene may be restricted in simulated flue gas because of competition from the inorganic components for the limited active sites. Bertinchamps et al. [54] have investigated the influence of NO on the performances of vanadium oxide based catalysts, and NO was shown to induce an increase in chlorobenzene conversion only if O₂ was present and conversion was maximized when catalyst contained W or Mo. The suggested reason for the positive enhancement effect is that NO can be oxidized to NO₂ which has higher oxidation power than O₂ and is able to assist O₂ in the reoxidation step of V⁴⁺O_x to V⁵⁺O_x, thus speeding up the oxidation cycle of catalyst. However, present research established that neither obvious competition effect nor positive effect of NO is observed on benzene catalytic oxidation at 400 °C: switching off the valves of NH₃, NO, HCl and SO₂ one by one barely enhances the removal efficiency of benzene. The results displayed in Table 3 indicate that catalytic reduction of benzene and NO_x apparently calls for different active sites on the catalysts. The disparity in effect of adding NO observed from this work and the reference [49], possibly ascribed to two reasons: (1) extremely low concentration (5 ppm) of benzene used in this work, which may not so susceptible to the reoxidation step of the VO_x phase (speeding up by the presence of NO); (2) the dependence of the thermodynamic equilibrium between NO and NO₂ on temperature can be considered. The results in Table 3 are

obtained when the test temperature was set at 400 °C. The oxidation of NO to NO₂ can be substantially restricted under this test temperature because of the thermodynamic equilibrium favors NO [49] and the remarkable decrease in NO₂ production could be a key factor to interpret the almost zero influence of NO here. Besides, a typical NO_x reduction of 90% was also observed during benzene destruction tests using VWNT at 300 °C. In conclusion, the present research demonstrates that V₂O₅–WO₃/TiO₂-based catalysts can achieve benzene removal effectively as well as high NO_x reduction.

3.3. Kinetics analysis

Each benzene catalytic oxidation test conducted in this study was under isothermal operation. The benzene catalytic oxidation reaction rate (r_B) in the presence of oxygen can be described as:

$$r_B = -kC_B^m C_{O_2}^n \quad (2)$$

where k is the rate constant for benzene catalytic oxidation; C_B represents the concentration of benzene (10 ppm) and C_{O_2} is the concentration of oxygen (5.0%). As $C_{O_2} >> C_B$ in the tests, C_{O_2} can be assumed to be constant. Moreover, catalytic oxidation was previously reported to be following the first order reaction [28], thus r_B can be expressed by Eq. (3).

$$r_B = -kC_B = \frac{dC_B}{dt} \quad (3)$$

The above equation can be integrated to

$$\ln\left(1 - \frac{\eta_b}{100}\right) = -kt \quad (4)$$

Therefore, the reaction rate constant k is calculated as:

$$k = -\frac{Q}{C_0 \times V} \times \ln\left(1 - \frac{\eta_b}{100}\right) \quad (5)$$

Q signifies the inlet molar flow rate of benzene (mol s⁻¹), C_0 represents the inlet concentration of benzene (mol cm⁻³), and V is the volume of the catalyst (cm³). Average removal efficiency of benzene η_b from a period of 5 min sampling was imported into Eq. (5).

The reaction rate constants of VWNT (k_{VWNT}), VWT1 (k_{VWT1}) and VWT2 (k_{VWT2}) in relatively low temperature region of 160–220 °C are listed in Table 4. From Table 4 it follows that reaction rate constants increase with the increasing reaction temperatures. Moreover, benzene catalytic oxidation over VWNT has the largest reaction rate constants in each reaction temperature comparing with those of other two catalysts, almost three or four times larger than that for VWT2. Large reaction rate constant for VWNT

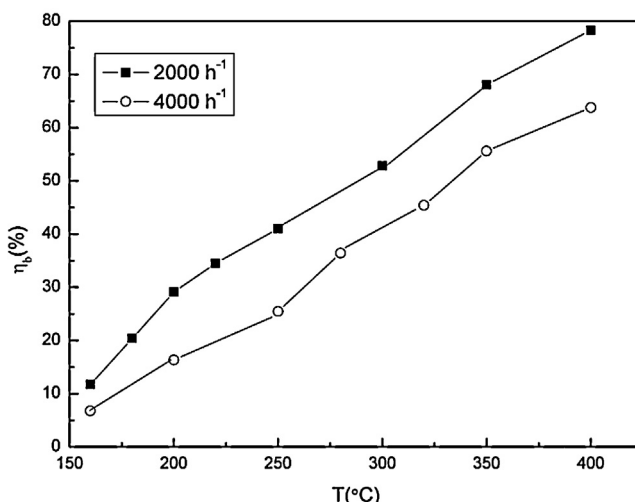


Fig. 9. Benzene removal efficiencies achieved with VWNT at different space velocities (initial concentration: 10 ppm; T: 350 °C).

Table 4

The reaction rate constants k of VWNT, VWT1 and VWT2 at different reaction temperatures.

Reaction temperature (°C)	k_{VWNT} (s ⁻¹)	k_{VWT1} (s ⁻¹)	k_{VWT2} (s ⁻¹)
160	0.14 ± 0.05	0.09 ± 0.05	0.04 ± 0.03
180	0.20 ± 0.06	0.11 ± 0.04	0.05 ± 0.04
200	0.30 ± 0.06	0.18 ± 0.16	0.09 ± 0.04
220	0.34 ± 0.06	0.22 ± 0.08	0.11 ± 0.04

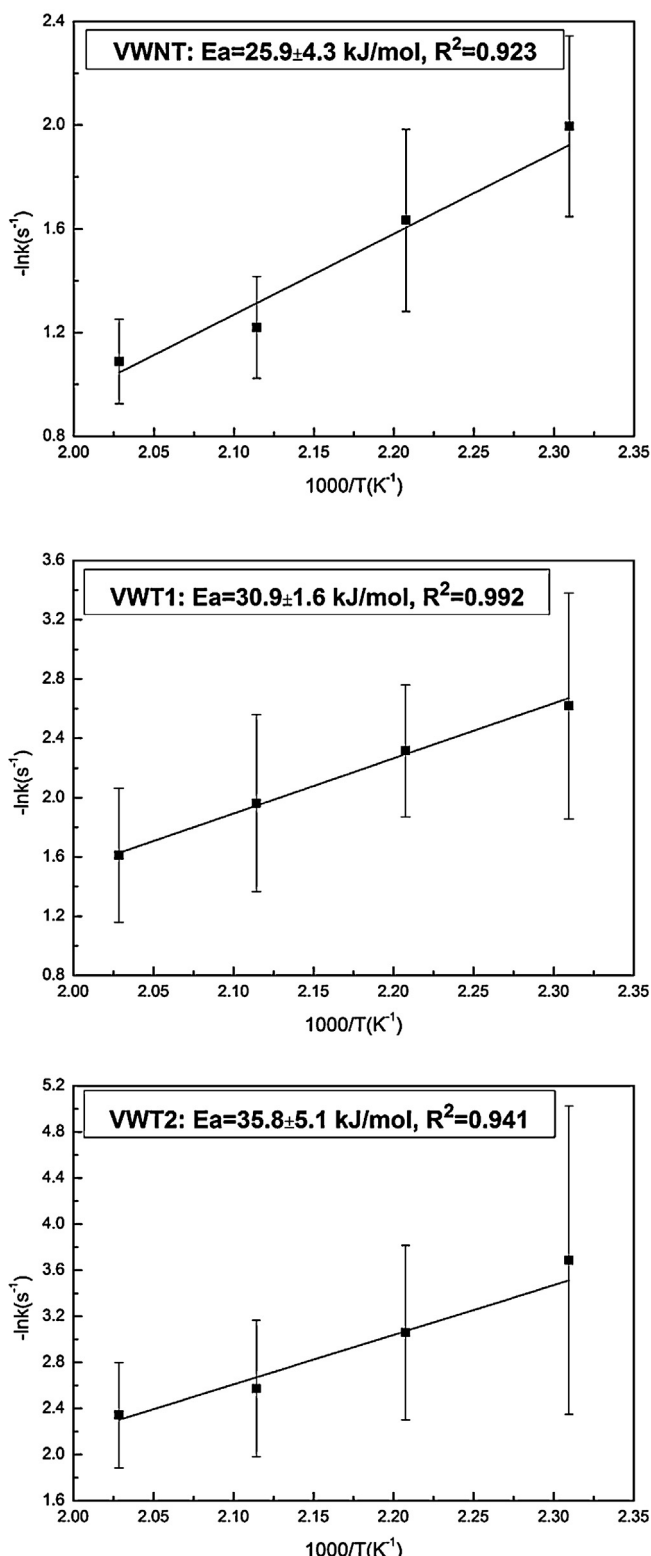


Fig. 10. Arrhenius plots obtained from VWNT, VWT1 and VWT2.

attributes to higher adsorption ability as well as higher catalytic activity of VWNT. The relationship between activation energy E_a and rate constant k can be expressed by the Arrhenius equation [15]:

$$\ln k = -\left(\frac{E_a}{RT}\right) + B \quad (6)$$

where R is gas constant (8.314 J/K mol); T is the gas temperature (K) and B is a constant. The apparent activation energy (E_a) is then obtained from the slope of the linear $-\ln k$ vs. $1000/T$ plot (slope = E_a/R).

As can be seen from Fig. 10, all the plots ($-\ln k$ vs. $1000/T$) exhibit good linearity according to the Arrhenius equation. The apparent activation energy for benzene catalytic oxidation performed by using the three catalysts can be deduced from the slopes of the linear $-\ln k$ vs. $1000/T$ plots (slope = E_a/R). The apparent activation energy for VWNT is 25.9 ± 4.3 kJ mol⁻¹, lower than those for VWT1 (30.9 ± 1.6 kJ mol⁻¹) and VWT2 (35.8 ± 5.1 kJ mol⁻¹), indicating the better catalytic performance of VWNT. On the other hand, different apparent activation energies determined for benzene oxidation over these three catalysts also suggest different reaction pathways occur on effective active sites. It appears that benzene catalytic oxidation is easier to occur on VWNT rather than on VWT1 and VWT2, which further confirms higher catalytic activity can be obtained when the nano-TiO₂ instead of conventional TiO₂ is applied as the catalyst support.

4. Conclusions

Catalytic oxidation of trace benzene (1–10 ppm) was carried out over honeycomb-shaped V₂O₅–WO₃/TiO₂-based catalysts in simulated flue gas. The on-line monitoring of benzene at these low concentrations was achieved through use of REMPI-TOFMS. Benzene catalytic removal efficiency is independent of V content under these experimental conditions, VWNT supported by nano-TiO₂ but with least V loading showed best catalytic activity, suggesting that not only the active transition metals content but also the catalyst support types determine the activity of the catalyst. Typical molecular structures of VO_x surface species with one terminal V=O bond and three Ti–O–V bonds connected to Ti support, were observed in the Raman spectra of VWNT, and are likely to be responsible for the enhanced activity observed for the catalyst. Increasing benzene inlet concentration from 1 to 10 ppm intensifies the competition among benzene molecules for active sites but still causes an unexpected increase in benzene catalytic removal efficiency for VWNT, due to the catalyst is possessing sufficient active sites. In addition, lowering inlet benzene concentration reduced the probability of collision between benzene molecules and the catalyst surface sites, reducing the organic pollutant removal efficiency. However, opposite trends were observed in VWT1 and VWT2, indicating their relatively poor catalytic activities. Catalytic removal efficiency decreased with increasing space velocity which is attributed to shorter benzene retention time on the catalyst as well as the reduction of the effective collisions between benzene molecules and catalytic active sites. The better performance of VWNT which is supported by nano-TiO₂ than those of the two catalysts which are supported by conventional TiO₂ can be attributed to the greater adsorption ability because of the catalyst with nano TiO₂ support has larger specific surface area and has more pores with the diameter close to the diameter of the benzene molecule. The presence of V=O and V–O–support bonds in VWNT is also making the higher catalytic activity of VWNT a reasonable suggestion. Pure anatase phase, instead of a mixture of anatase and rutile phases, observed in the support of VWNT may be another reason for its better performance. Excessive impurities, introduced into monolithic catalyst during its preparation in the form of additives, may increase the risk of reducing catalytic activity by squeezing out the catalyst active ingredients. Neither positive enhancement effect nor negative competition effect between benzene removal and other components in the flue gas was observed, suggesting that organic compounds can be removed effectively over V₂O₅–WO₃/TiO₂-based catalysts in combination with NO_x reduction. Reaction rate

constant for benzene catalytic oxidation measured for VWNT is the largest one at each the reaction temperature tested. Furthermore, the activated energy required for benzene catalytic oxidation determined for VWNT is the lowest, another indication for the better performance of VWNT.

Acknowledgments

The Project is supported by the Major State Basic Research Development Program of China (2011CB201500), the National Natural Science Foundation of China (51276162) and the Program of Introducing Talents of Discipline to University (B08026). Thanks for the experimental testing and data analysis support from the internship student, Mr. Jeremy Lecomte (Universite de Orleans, France, student intern at U.S. EPA).

The views expressed in this publication are those of the individual authors and do not necessarily reflect the views and policies of the U.S. Environmental Protection Agency (EPA). Scientists in EPA's Office of Research and Development have prepared the EPA sections, and those sections have been reviewed in accordance with EPA's peer and administrative review policies and approved for publication. Mention of trade names or commercial products does not constitute endorsement or recommendation for use.

References

- [1] T.F. Garetto, M.S. Avila, C.I. Vignatti, V.V. Rao, K. Chary, C.R. Apesteguía, *Catal. Lett.* 130 (2009) 476–480.
- [2] H. Einaga, S. Futamura, *J. Catal.* 227 (2004) 304–312.
- [3] H. Hagenmaier, K. Horch, H. Fahlenkamp, G. Schetter, *Chemosphere* 23 (1991) 1429–1437.
- [4] M. Hiraoka, N. Takeda, T. Kasakura, Y. Imoto, H. Tsuboi, T. Iwasaki, *Chemosphere* 23 (1991) 1445–1457.
- [5] R. Weber, T. Sakurai, H. Hagenmaier, *Appl. Catal. B* 20 (1999) 249–256.
- [6] H. Hagenmeier, *VDI Berichte* 730 (1989) 239–254.
- [7] B.M. Weckhuysen, I.E. Wachs, G. Deo, A. Andreini, M.A. Vuurman, M. de Boer, M.D. Amiridis, *J. Catal.* 161 (1996) 211–221.
- [8] Y. Ide, K. Kashiwabara, K. Okada, S. Mori, M. Hara, *Chemosphere* 32 (1996) 189–198.
- [9] K. Everaert, J. Baeyens, *J. Hazard. Mater.* B109 (2004) 113–139.
- [10] S. Krishnamoorthy, J.P. Baker, M.D. Amiridis, *Catal. Today* 40 (1998) 39–46.
- [11] R. Weber, T. Sakurai, *Appl. Catal. B* 34 (2001) 113–127.
- [12] G. Wielgośiński, A. Grochowski, T. Machej, T. Pająk, W. Ćwiąkalski, *Chemosphere* 67 (2007) S150–S154.
- [13] S. Albionetti, J.E. Mengou, F. Trifiro, *Catal. Today* 119 (2007) 295–300.
- [14] D. Shin, S. Choi, J.-E. Oh, Y.-S. Chang, *Environ. Sci. Technol.* 33 (1999) 2657–2666.
- [15] C.C. Yang, S.H. Chang, B.Z. Hong, K.H. Chi, M.B. Chang, *Chemosphere* 73 (2008) 890–895.
- [16] C. Cho, S. Ihm, *Environ. Sci. Technol.* 36 (2002) 1600–1606.
- [17] S. Krishnamoorthy, J.A. Rivas, M.D. Amiridis, *J. Catal.* 193 (2000) 264–272.
- [18] P. Liljelind, J. Unsworth, O. Maaskant, S. Marklund, *Chemosphere* 42 (2001) 615–623.
- [19] E. Finocchio, G. Busca, M. Notaro, *Appl. Catal. B* 62 (2006) 12–20.
- [20] H. Einaga, S. Futamura, *React. Kinet. Catal. Lett.* 81 (2004) 121–128.
- [21] X.Y. Fan, H.S. Yang, W. Tian, A.M. Nie, T.F. Hou, F.M. Qiu, X.B. Zhang, *Catal. Lett.* 141 (2011) 158–162.
- [22] A.M. Nie, H.S. Yang, Q. Li, X.Y. Fan, F.M. Qiu, X.B. Zhang, *Ind. Eng. Chem. Res.* 50 (2011) 9944–9948.
- [23] E. Finocchio, M. Baldi, G. Busca, C. Pistarino, G. Romezzano, F. Bregani, G.P. Toledo, *Catal. Today* 59 (2000) 261–268.
- [24] J. Lichtenberger, M.D. Amiridis, *J. Catal.* 223 (2004) 296–308.
- [25] G. Busca, M. Baldi, C. Pistarino, J.M. Gallardo Amores, V. Sanchez Escribano, E. Finocchio, G. Romezzano, F. Bregani, G.P. Toledo, *Catal. Today* 53 (1999) 525–533.
- [26] H. Einaga, A. Ogata, *J. Hazard. Mater.* 164 (2009) 1236–1241.
- [27] H.C. Wang, S.H. Chang, P.C. Hung, J.F. Hwang, M.B. Chang, *Chemosphere* 71 (2008) 388–397.
- [28] H.C. Wang, H.S. Liang, M.B. Chang, *J. Hazard. Mater.* 186 (2011) 1781–1787.
- [29] U. Boesl, R. Zimmermann, C. Weickhardt, D. Lenoir, K.W. Schramm, A. Kettrup, E.W. Schlag, *Chemosphere* 29 (1994) 1429–1440.
- [30] H. Oser, R. Thanner, H.H. Grotheer, *Chemosphere* 37 (1998) 2361–2374.
- [31] J. Velazquez, L.A. Voloboueva, T.A. Cool, *Combust. Sci. Technol.* 134 (1998) 139–163.
- [32] Q. Li, H.S. Yang, A.M. Nie, X.Y. Fan, X.B. Zhang, *Catal. Lett.* 141 (2011) 1237–1242.
- [33] M. Hunger, J. Weitkamp, *Angew. Chem. Int.* 40 (2001) 2954–2971.
- [34] X. Gao, I.E. Wachs, *J. Phys. Chem. B* 104 (2000) 1261–1268.
- [35] M.V. Martínez-Huerta, X. Gao, H. Tian, I.E. Wachs, J.L.G. Fierro, M.A. Bañares, *Catal. Today* 118 (2006) 279–287.
- [36] D.E. Keller, T. Visser, F. Soulimani, D.C. Koningsberger, B.M. Weckhuysen, *Vib. Spectrosc.* 43 (2007) 140–151.
- [37] G.T. Went, S.T. Oyama, A.T. Bell, *J. Phys. Chem.* 94 (1990) 4240–4246.
- [38] Q. Li, H. Yang, F. Qiu, X. Zhang, *J. Hazard. Mater.* 192 (2011) 915–921.
- [39] C.B. Wang, G. Deo, I.E. Wachs, *J. Catal.* 178 (1998) 640–648.
- [40] D.A. Bulushev, L. Kiwi-Minsker, F. Rainone, A. Renken, *J. Catal.* 205 (2002) 115–122.
- [41] N. Magg, B. Immaraporn, J.B. Giorgi, T. Schroeder, M. Bäumer, J. Döbler, Z. Wu, E. Kondratenko, M. Cherian, M. Baerns, P.C. Stair, J. Sauer, H. Freund, *J. Catal.* 226 (2004) 88–100.
- [42] B.M. Weckhuysen, D.E. Keller, *Catal. Today* 78 (2003) 25–46.
- [43] M.A. Reiche, M. Maciejewski, A. Baiker, *Catal. Today* 56 (2000) 347–355.
- [44] L. Chen, J. Li, M. Ge, *J. Phys. Chem. C* 113 (2009) 21177–21184.
- [45] B. Schimmoeller, R. Delaigle, D.P. Debecker, E.M. Gaigneaux, *Catal. Today* 157 (2010) 198–203.
- [46] L.J. Burcham, G. Deo, X. Gao, I.E. Wachs, *Top. Catal.* 11/12 (2000) 85–100.
- [47] L.J. Burcham, I.E. Wachs, *Catal. Today* 49 (1999) 467–484.
- [48] I.E. Wachs, *Catal. Today* 27 (1996) 437–455.
- [49] K. Fogar, J.R. Anderson, *Appl. Catal.* 23 (1986) 139–155.
- [50] J. Zhang, M. Li, Z. Feng, J. Chen, C. Li, *J. Phys. Chem. B* 110 (2006) 927–935.
- [51] J. Zhu, W. Zheng, B. He, J. Zhang, M. Anpo, *J. Mol. Catal. A* 216 (2004) 35–43.
- [52] A.M. Mastral, T. García, M.S. Callén, M.V. Navarro, J. Galbán, *Energy Fuels* 15 (2001) 1–7.
- [53] R. Murillo, T. García, E. Aylón, M.S. Callén, M.V. Navarro, J.M. López, A.M. Mastral, *Carbon* 42 (2004) 2009–2017.
- [54] F. Bertinchamps, M. Treinen, N. Blangenois, E. Mariage, E.M. Gaigneaux, *J. Catal.* 230 (2005) 493–498.